

PAPER

## *Ab initio* thermodynamics of carbon segregation on dislocation cores in bcc iron

To cite this article: B Lüthi *et al* 2019 *Modelling Simul. Mater. Sci. Eng.* **27** 074002

View the [article online](#) for updates and enhancements.



**IOP | ebooks™**

Bringing you innovative digital publishing with leading voices to create your essential collection of books in STEM research.

Start exploring the collection - download the first chapter of every title for free.

# ***Ab initio* thermodynamics of carbon segregation on dislocation cores in bcc iron**

**B Lüthi<sup>1</sup>, F Berthier<sup>2</sup> , L Ventelon<sup>1</sup> , B Legrand<sup>1</sup>,  
D Rodney<sup>3</sup> and F Willaime<sup>4</sup>**

<sup>1</sup> DEN-Service de Recherches de Métallurgie Physique, CEA, Université Paris-Saclay, F-91191 Gif-sur-Yvette, France

<sup>2</sup> Synthèse, Propriétés et Modélisation des Matériaux (SP2M)/Institut de Chimie Moléculaire et des Matériaux d'Orsay (ICMMO), CNRS-Université Paris Sud, UMR 8182, Université Paris-Saclay, F-91405 Orsay Cedex, France

<sup>3</sup> Institut Lumière Matière, CNRS-Université Claude Bernard Lyon 1, F-69622 Villeurbanne, France

<sup>4</sup> DEN-Département des Matériaux pour le Nucléaire, CEA, Université Paris-Saclay, F-91191 Gif-sur-Yvette, France

E-mail: [lisa.ventelon@cea.fr](mailto:lisa.ventelon@cea.fr)

Received 21 February 2019, revised 26 May 2019

Accepted for publication 11 June 2019

Published 8 July 2019



CrossMark

## **Abstract**

The equilibrium segregation of carbon atoms in the core of screw dislocations in body-centred cubic Fe is modelled using a generalized Ising model parametrized on density functional theory calculations and solved using both mean-field calculations and Monte Carlo simulations. Recently, a strong carbon-dislocation attraction was evidenced, resulting in a spontaneous reconstruction of the dislocation core towards a hard core configuration, where the carbon atom is located at the centre of a regular trigonal prism called a prismatic site. Here we show that the fourth neighbour octahedral sites of the reconstructed core are also attractive for carbon with a binding energy similar to that of the prismatic core site reported previously. This suggests that the dislocation may be decorated by lines of carbon atoms on both types of sites. Moreover, all carbon-carbon interactions including intra-line and inter-line interactions, are found repulsive. Segregation therefore results from a competition between the dislocation-carbon attraction and the carbon-carbon repulsion, leading to complex ordering phenomena that are analysed here in detail. Notably, we evidence a high temperature regime, in the regime of dynamical strain ageing of steels, where the prismatic line is half-occupied on average with every other prismatic site occupied by a carbon atom while the octahedral lines are empty. The iso-concentrations for the prismatic and octahedral lines obtained with the mean-field approach and with Monte Carlo simulations are qualitatively similar.

Keywords: DFT calculations, dislocation-solute interaction, bcc iron, mean-field calculations, Monte Carlo simulations

(Some figures may appear in colour only in the online journal)

## 1. Introduction

The marked temperature and strain-rate dependence of the yield stress at low temperatures in body-centred cubic (bcc) metals has received considerable attention in the literature (Hirth and Lothe 1982, Christian 1983). In particular the role of the core structure of the  $1/2\langle 111 \rangle$  screw dislocation on this unconventional low-temperature plastic behaviour has been investigated (Vitek 1974). However, the fundamental understanding of the contribution due to the concentration of an alloying addition element close to the dislocation core remains virtually unexplored. In this paper we investigate the complex variations with temperature of the solute segregation on different dislocation core sites in the Fe(C) system, based on density functional theory (DFT) electronic structure calculations.

The segregation of solute atoms to dislocation lines is a phenomenon central to solid-solution hardening. It was first analysed theoretically in the seminal work of Cottrell and Bilby (1949). Recent works have focused on predictions via elasticity theory, interatomic potentials and Monte Carlo simulations (see e.g. Veiga *et al* 2011, 2015, Chockalingam *et al* 2014, Waseda *et al* 2017). However, these approaches remain limited in their ability to predict segregation profiles near dislocation cores because elasticity cannot be applied in this region and interatomic potentials are of limited predictability with respect to the detailed structure of dislocation cores.

Using DFT calculations, it was recently shown that  $1/2\langle 111 \rangle$  screw dislocation cores can reconstruct in presence of interstitial solute atoms in bcc metals (Ventelon *et al* 2015, Lüthi *et al* 2017, Rodney *et al* 2017). First considering carbon solutes, a strong attractive interaction was evidenced in Fe, Mo and W, inducing a spontaneous reconstruction of the core structure towards a low-energy configuration where, unexpectedly, the dislocation core adopts a hard-core configuration. The carbon atoms are then at the centre of regular trigonal prisms formed by the metal atoms inside the dislocation core. The affinity of carbon atoms for these prismatic sites can be related to the similarity with their local environment in Fe<sub>3</sub>C cementite and in WC and MoC hexagonal carbides (Lüthi *et al* 2017). The same core reconstruction was obtained with other octahedral interstitial solutes (B, N, O) in Fe (Lüthi *et al* 2018), whereas a different behaviour was observed for C in V, Nb and Ta (Lüthi *et al* 2017).

Considering the Fe(C) system at thermal equilibrium, the strongly attractive dislocation-carbon interaction was shown, using a simple mean field model, to lead to a core saturation by carbon atoms at room temperature, even for very low carbon bulk concentrations (Ventelon *et al* 2015). However, this first study considered only carbon segregation on the prismatic sites at the very core of the dislocation. In the present paper, we expand this study to include a broader set of sites likely to attract carbon atoms. We calculate the binding energies to these sites and the relevant interactions between carbon atoms using DFT calculations. Based on these *ab initio* data, we propose a pair interaction model and define an Ising Hamiltonian on an effective lattice. Using this Hamiltonian, we perform both mean-field calculations and Monte Carlo simulations in order to describe the temperature dependence of the carbon concentration in these different sites near the dislocation core. We evidence complex ordering phenomena that we analyse in detail.

## 2. Methodology

### 2.1. Calculations of the interactions based on DFT

We perform spin-polarized DFT calculations with the VASP code (Kresse and Furthmüller 1996) using the projector augmented wave pseudopotential scheme (Blöchl 1994, Kresse and Joubert 1999) within the Perdew–Burke–Ernzerhof generalized gradient approximation and a 400 eV kinetic-energy cutoff. We use a pseudopotential without semicore electrons for Fe and a pseudopotential with 2s and 2p valence states for C. All calculations are performed at constant cell volume with a 0.2 eV Hermite Gaussian broadening. Atomic positions are relaxed with a convergence criterion on forces of  $10^{-2}$  eV Å<sup>-1</sup>. For the dislocation calculations, we consider a quadrupolar periodic array of dislocation dipoles (see Ventelon *et al* 2013 for details about the cell geometry), with carbon atoms separated by either  $1b$  or  $2b$  along the  $\langle 111 \rangle$  direction of the dislocation line ( $b$  is the dislocation Burgers vector). We use a  $1 \times 2 \times 8$  shifted  $k$ -point grid with a cell size along the dislocation line of  $2b$ , resulting in 270 Fe atoms in the simulation cell. The calculations of interstitial carbon atoms in a perfect bcc crystal without dislocation are performed in a 250-atom cubic cell using a  $4 \times 4 \times 4$  shifted  $k$ -point grid.

The dislocation dipole is first relaxed in its easy core configuration, which is the minimum energy dislocation position in pure bcc metals (Rodney *et al* 2017). Then one carbon atom is introduced in an octahedral-like interstitial position, first nearest neighbour to one of the dislocations of the dipole, and the atomic positions are relaxed again. As explained in previous articles (Ventelon *et al* 2015, Lüthi *et al* 2017, 2018), this results in a reconstruction of the dislocation core towards a hard core configuration, which is unstable in pure bcc metals (Rodney *et al* 2017). The carbon atom is located at the centre of a regular trigonal prism formed by the iron atoms inside the dislocation core, which is called hereafter a prismatic site. For a distance between carbon atoms along the dislocation line of  $1b$  (resp.  $2b$ ), this configuration is denoted  $P_{1b}$  (resp.  $P_{2b}$ ). Note that in these calculations, the other dislocation of the dipole remains on its easy core configuration.

We then investigate the segregation of carbon in octahedral-like interstitial sites  $i$ th nearest neighbours to the reconstructed dislocation core. These sites are denoted  $O^{(i)}$  with  $i$  ranging from 1 to 6. Starting with the  $P_{2b}$  configuration, i.e. with every other prismatic site along the dislocation occupied by a carbon atom, our DFT calculations show that: (i) a carbon atom on a  $O^{(1)}$  site decays into the empty prismatic site upon relaxation, resulting in the  $P_{1b}$  configuration; (ii) the configurations obtained when a carbon atom is placed either on a  $O^{(2)}$  or on a  $O^{(6)}$  site are locally stable but with repulsive interaction energies; (iii) a carbon atom placed either on a  $O^{(3)}$  or on a  $O^{(5)}$  site decays into a  $O^{(4)}$  site; (iv) the configuration obtained starting from the  $O^{(4)}$  site, denoted  $P_{2b} + O^{(4)}$ , is stable with an attractive dislocation-carbon interaction energy of about  $-0.4$  eV, taking as reference the  $P_{2b}$  configuration. This binding energy is similar to that of the  $P_{1b}$  configuration taking as reference the same  $P_{2b}$  configuration, i.e. from a  $P_{2b}$  configuration, it is energetically equivalent to place a carbon atom either in an empty prismatic site to form a  $P_{1b}$  configuration, or in a  $O^{(4)}$  site to form a  $P_{2b} + O^{(4)}$  configuration. There are six equivalent  $O^{(4)}$  sites around the reconstructed core, denoted hereafter  $O_k^{(4)}$ ,  $k = 1$  to 6, as represented in figure 1.

On the basis of the above results, we develop an Ising Hamiltonian, which takes into account both the prismatic ( $P$ ) sites inside the dislocation core and the six different  $O^{(4)}$  sites around the reconstructed core:

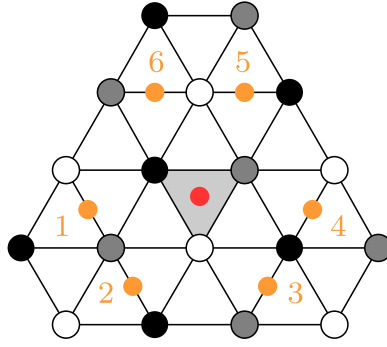


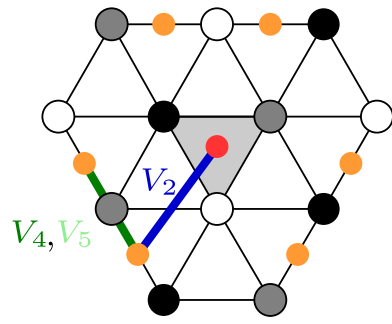
**Figure 1.** Projection on the (111) plane of the iron (in white, black and grey) and carbon (in colour) atomic positions around the reconstructed dislocation core (represented by a grey triangle). The prismatic site  $P$  inside the hard core is represented with a red circle while the  $O_k^{(4)}$  sites, with  $k$  ranging from 1 to 6, are represented by orange circles.

$$H = \sum_i \Delta E_i^{\text{seg},0} \sigma_i + \frac{1}{2} \sum_{i,j \neq i} V_{ij} \sigma_i \sigma_j \quad (1)$$

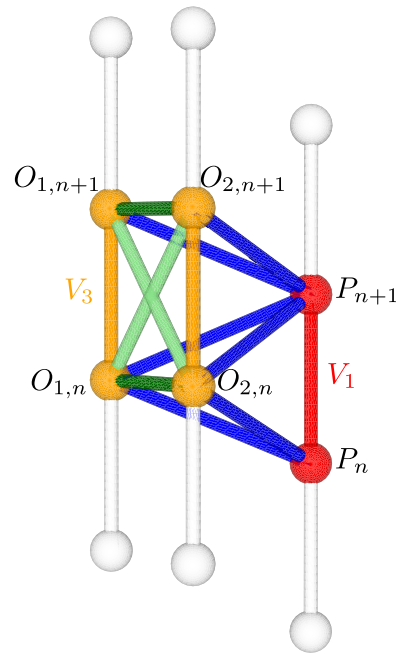
with  $\Delta E_i^{\text{seg},0}$  the segregation energy on site  $i$  ( $P$  or  $O^{(4)}$  sites) in the dilute limit and  $V_{ij}$  the pair interaction between carbon atoms on sites  $i$  and  $j$ .  $\sigma_i$  is the site occupancy such that  $\sigma_i = 1$  if site  $i$  is occupied by a carbon atom and  $\sigma_i = 0$  otherwise. DFT calculations show that carbon-carbon interactions are short-ranged and can be limited to first neighbours. This allows to reduce the number of interaction terms  $V_{ij}$  to only five non-equivalent terms that are illustrated in figure 2. First, interactions between  $P$  sites can be limited to first-neighbour sites, with an interaction term  $V_{PP} \equiv V_1$ . Also, as illustrated in figure 2(b),  $O^{(4)}$  sites are contained in (111) planes halfway between  $P$  sites. Therefore, still limiting the interactions to first neighbours, a given  $P$  site interacts with twelve  $O^{(4)}$  sites that are all equivalent by symmetry. The corresponding interaction term is noted  $V_{PO^{(4)}} \equiv V_2$ . Concerning interactions between  $O^{(4)}$  sites, we have to distinguish between sites in the same or different (111) planes (figure 2(b)). This is done by using a  $\sim$  symbol on one of  $O^{(4)}$  sites when the sites are in different (111) planes. Three configurations are then possible because of symmetry. First, first-neighbour  $O^{(4)}$  sites parallel to the dislocation line interact in a way similar to  $P$  sites, with an interaction term  $V_{O^{(4)}\widetilde{O^{(4)}}} \equiv V_3$ . Then,  $O^{(4)}$  sites in a given (111) plane form three equivalent pairs of close neighbours, (1, 2), (3, 4) and (5, 6) using the notations of figure 1. Carbon atoms forming such pairs interact with an interaction term  $V_{O^{(4)}O^{(4)}} = V_{O_1^{(4)}O_2^{(4)}} = V_{O_3^{(4)}O_4^{(4)}} = V_{O_5^{(4)}O_6^{(4)}} \equiv V_4$ . The third non-negligible interaction term corresponds to  $O^{(4)}$  sites inside a close pair, for instance (1, 2), but on different (111) planes, with an interaction term  $V_{O^{(4)}\widetilde{O^{(4)}}} = V_{O_1^{(4)}\widetilde{O_2^{(4)}}} = V_{O_3^{(4)}\widetilde{O_4^{(4)}}} = V_{O_5^{(4)}\widetilde{O_6^{(4)}}} \equiv V_5$ . We have checked through the DFT calculations discussed below that all other interactions, which involve more distant neighbours, such as  $V_{O_1^{(4)}O_4^{(4)}}$ ,  $V_{O_1^{(4)}O_5^{(4)}}$  or  $V_{O_1^{(4)}O_6^{(4)}}$ , are below 0.1 eV and will be neglected in the following.

The seven parameters of the Hamiltonian ( $\Delta E_P^{\text{seg},0}$ ,  $\Delta E_{O^{(4)}}^{\text{seg},0}$  and  $V_1$ – $V_5$ ) are fitted to DFT calculations of the total binding energies, defined by:

$$E_b^{\text{DFT}} = E_{\text{dislo}+nC} - E_{\text{dislo}} - n(E_C - E_{\text{bulk}}) \quad (2)$$



(a)



(b)

**Figure 2.** Schematic representation of the carbon–carbon interactions between  $P$  and  $O^{(4)}$  sites: (a) in projection along the Burgers vector direction and (b) in perspective perpendicular to the Burgers vector. The interaction terms  $V_1$ ,  $V_2$ ,  $V_3$ ,  $V_4$  and  $V_5$  are represented in red, blue, orange, dark green and light green, respectively.

with  $E_{\text{dislo}+n_C}$ , the energy of a cell containing a reconstructed dislocation and  $n$  carbon atoms in prismatic and/or  $O^{(4)}$  interstitial sites. The dislocation reference state is always the energy of a simulation cell containing a hard dislocation core (the other dislocation of the dipole remaining in its easy core configuration) without any carbon, denoted  $E_{\text{dislo}}$ .  $E_{\text{bulk}}$  (resp.  $E_C$ ) corresponds to the energy of a bcc cubic cell with no carbon atom (resp. with one carbon atom in an octahedral site).

**Table 1.** Total binding energies (in eV) calculated with DFT and using the Ising model, and corresponding relative errors  $\Delta E/\langle E \rangle$  (in %) for different  $P + O^{(4)}$  configurations. The ten first configurations are used to fit the Ising model and the following configurations are used to test the validity of the model. When several  $O_i^{(4)}$  sites are occupied, the carbon atoms are placed in the same (111) plane unless a  $\sim$  symbol is indicated. In that case, the corresponding carbon atom is positioned in the (111) plane just above (or equivalently below) the plane containing the other carbon atom(s).

Configuration	$E_b^{\text{DFT}}$	$E_b^{\text{model}}$	Error
$P_{1b}$	-1.24	-1.24	0
$P_{2b}$	-0.84	-0.84	0
$P_{1b} + O_1^{(4)}$	-1.52	-1.53	0.7
$P_{2b} + O_1^{(4)}$	-1.23	-1.24	0.8
$P_{2b} + O_1^{(4)} + \widetilde{O_1^{(4)}}$	-1.04	-1.04	0
$P_{2b} + \widetilde{O_3^{(4)}} + O_4^{(4)}$	-1.22	-1.23	0.8
$P_{2b} + \widetilde{O_3^{(4)}} + O_4^{(4)}$	-0.80	-0.82	2.5
$P_{2b} + O_1^{(4)} + O_4^{(4)}$	-1.55	-1.64	5.6
$P_{2b} + O_1^{(4)} + O_5^{(4)}$	-1.64	-1.64	0
$P_{2b} + O_4^{(4)} + O_5^{(4)}$	-1.59	-1.64	3.1
$P_{1b} + O_1^{(4)} + \widetilde{O_1^{(4)}}$	-1.32	-1.22	7.9
$P_{1b} + O_1^{(4)} + \widetilde{O_4^{(4)}}$	-1.78	-1.82	2.2
$P_{1b} + O_1^{(4)} + O_5^{(4)}$	-1.86	-1.82	2.2
$P_{2b} + O_5^{(4)} + O_6^{(4)}$	-1.29	-1.23	4.8
$P_{2b} + \widetilde{O_5^{(4)}} + \widetilde{O_6^{(4)}}$	-1.00	-0.82	19.8
$P_{2b} + O_1^{(4)} + \widetilde{O_4^{(4)}}$	-1.57	-1.64	4.4
$P_{2b} + O_1^{(4)} + \widetilde{O_5^{(4)}}$	-1.60	-1.64	2.5
$P_{2b} + O_1^{(4)} + O_5^{(4)} + O_6^{(4)}$	-1.63	-1.63	0
$P_{2b} + O_1^{(4)} + \widetilde{O_3^{(4)}} + O_5^{(4)}$	-1.98	-2.04	3.0
$P_{2b} + O_1^{(4)} + \widetilde{O_3^{(4)}} + O_5^{(4)}$	-2.02	-2.04	1.0
$P_{2b} + O_1^{(4)} + O_4^{(4)} + \widetilde{O_5^{(4)}}$	-1.90	-2.04	7.1
$P_{2b} + O_1^{(4)} + \widetilde{O_4^{(4)}} + \widetilde{O_5^{(4)}}$	-1.80	-2.04	12.5
$P_{2b} + O_1^{(4)} + \widetilde{O_3^{(4)}} + O_4^{(4)} + O_5^{(4)}$	-1.45	-1.62	11.1
$P_{2b} + O_1^{(4)} + \widetilde{O_3^{(4)}} + O_4^{(4)} + \widetilde{O_5^{(4)}}$	-1.37	-1.62	16.7

Table 1 summarizes the total binding energies of the investigated configurations calculated with DFT and used for the fitting and validation procedures. In these configurations, one or two carbon atoms are first positioned in  $P$  sites, resulting in either a  $P_{1b}$  or a  $P_{2b}$  configuration. Then an additional carbon atom is positioned in a  $O^{(4)}$  site, forming a  $P_{1b} + O_i^{(4)}$  or  $P_{2b} + O_i^{(4)}$  configuration. Other configurations are generated by adding another carbon atom in a different  $O^{(4)}$  site, forming  $P_{1b} + O_i^{(4)} + O_j^{(4)}$  and  $P_{2b} + O_i^{(4)} + O_j^{(4)}$  configurations. It may be observed that this last carbon atom can be introduced either in the same (111) plane as  $O_i^{(4)}$  or in the (111) plane just above or below (figure 2(b)). The ten first configurations in table 1 are used to adjust the parameters of the Ising model. The binding energies are expressed as:

$$\begin{aligned}
E_b^{\text{DFT}}(P_{1b}) &= 2\Delta E_P^{\text{seg},0} + 2V_1 \\
E_b^{\text{DFT}}(P_{2b}) &= \Delta E_P^{\text{seg},0} \\
E_b^{\text{DFT}}(P_{1b} + O_1^{(4)}) &= 2\Delta E_P^{\text{seg},0} + \Delta E_{O_1^{(4)}}^{\text{seg},0} + 2V_1 + 2V_2 \\
E_b^{\text{DFT}}(P_{2b} + O_1^{(4)}) &= \Delta E_P^{\text{seg},0} + \Delta E_{O_1^{(4)}}^{\text{seg},0} + V_2 \\
E_b^{\text{DFT}}(P_{2b} + O_1^{(4)} + \widetilde{O_1^{(4)}}) &= \Delta E_P^{\text{seg},0} + 2\Delta E_{O_1^{(4)}}^{\text{seg},0} + 2V_2 + V_3 \\
E_b^{\text{DFT}}(P_{2b} + O_3^{(4)} + O_4^{(4)}) &= \Delta E_P^{\text{seg},0} + 2\Delta E_{O_3^{(4)}}^{\text{seg},0} + 2V_2 + V_4 \\
E_b^{\text{DFT}}(P_{2b} + \widetilde{O_3^{(4)}} + O_4^{(4)}) &= \Delta E_P^{\text{seg},0} + 2\Delta E_{O_3^{(4)}}^{\text{seg},0} + 2V_2 + 2V_5 \\
E_b^{\text{DFT}}(P_{2b} + O_1^{(4)} + O_4^{(4)}) &= \Delta E_P^{\text{seg},0} + 2\Delta E_{O_1^{(4)}}^{\text{seg},0} + 2V_2 \\
E_b^{\text{DFT}}(P_{2b} + O_1^{(4)} + O_5^{(4)}) &= \Delta E_P^{\text{seg},0} + 2\Delta E_{O_1^{(4)}}^{\text{seg},0} + 2V_2 \\
E_b^{\text{DFT}}(P_{2b} + O_4^{(4)} + O_5^{(4)}) &= \Delta E_P^{\text{seg},0} + 2\Delta E_{O_4^{(4)}}^{\text{seg},0} + 2V_2.
\end{aligned} \tag{3}$$

The set of parameters thus obtained is:  $\Delta E_P^{\text{seg},0} = -0.84$  eV,  $\Delta E_{O_1^{(4)}}^{\text{seg},0} = -0.51$  eV,  $V_1 = 0.22$  eV,  $V_2 = 0.11$  eV,  $V_3 = 0.30$  eV,  $V_4 = 0.41$  eV and  $V_5 = 0.41$  eV.

The set of parameters is tested on several configurations and the comparison between total binding energies calculated from DFT and derived from the Ising model is given in table 1. The energies given by the Ising model are very close to the DFT values. The most important differences are obtained when several interaction terms are neglected in the Ising model, as in the case of the  $P_{2b} + O_1^{(4)} + \widetilde{O_1^{(4)}} + O_4^{(4)} + \widetilde{O_5^{(4)}}$  configuration, where the  $V_{O_1^{(4)}O_4^{(4)}}$ ,  $V_{O_1^{(4)}O_5^{(4)}}$  and  $V_{O_4^{(4)}O_5^{(4)}}$  interactions are neglected. The  $P_{2b} + O_5^{(4)} + O_6^{(4)}$  and  $P_{2b} + O_3^{(4)} + O_4^{(4)}$  configurations being equivalent by symmetry for an isolated dislocation, the 0.07 eV difference between the DFT results for these two configurations arises from the dipole geometry of the simulation cell, which breaks the symmetry.

## 2.2. Mean-field approximation

In order to determine the iso-concentrations (i.e. the site concentrations as a function of temperature for a given bulk concentration), we first perform mean field calculations. Mean-field modelling has several advantages: it allows to test the whole range of temperature and concentration very quickly and it is analytical, which allows to analyse the driving forces.

The interaction energies between two carbon atoms belonging to the same line are strongly repulsive ( $V_1, V_3 > 0$ ). Thus, one has to consider an ordering within each line. Given the fact that the inter-line interaction energies are also repulsive ( $V_2, V_4, V_5 > 0$ ), the ground state may be complex and the determination of the relevant sub-lattices is delicate. Thus we chose to use a mean-field algorithm per site for a large number of sites (see below), instead of a mean field per class of sites that requires to define sub-lattices beforehand.

In the mean-field approximation, the occupation of the different sites is obtained from the free energy minimization, which leads to the following equations (Fowler and Guggenheim 1960, Creuze *et al* 2000):

$$\frac{c_{P_n}}{1 - c_{P_n}} = \frac{c_{\text{bulk}}}{1 - c_{\text{bulk}}} \exp - \frac{\Delta E^{\text{seg}}(P_n)}{k_B T} \tag{4}$$



$$\frac{c_{O_{i,n}}^{(4)}}{1 - c_{O_{i,n}}^{(4)}} = \frac{c_{\text{bulk}}}{1 - c_{\text{bulk}}} \exp - \frac{\Delta E^{\text{seg}}(O_{i,n}^{(4)})}{k_B T}, \quad (5)$$

where  $k_B$  is the Boltzmann constant and the segregation energy  $\Delta E^{\text{seg}}(P_n)$  (resp.  $\Delta E^{\text{seg}}(O_{i,n}^{(4)})$ ) is the energy difference between a final configuration, where the carbon atom is located on site  $n$  of the  $P$  line (resp.  $O_i^{(4)}$  line) and an initial configuration, where the atom is in a bulk interstitial site. Note that each site has its own equation in the mean field per site approach. The six  $O^{(4)}$  lines are coupled two by two (via  $V_4$  and  $V_5$ ) and each pair  $(O_i^{(4)}, O_j^{(4)})$  is not directly coupled to the four other lines. It is thus possible to consider only the prismatic line and a pair of two  $O^{(4)}$  lines, for instance  $O_1^{(4)}$  and  $O_2^{(4)}$ . The system is then described using three lines of 100 sites and periodic boundary conditions, totalling 300 equations and as many variables,  $c_{P,n}$  for the  $P$  line and  $c_{O_{1,n}}^{(4)}$  and  $c_{O_{2,n}}^{(4)}$  with  $n$  the site index on the line ( $1 \leq n \leq 100$ ). Then, given the fact that site  $O_{1,n}^{(4)}$  lies in-between  $P_n$  and  $P_{n+1}$  (see figure 2(b)), the segregation energies for site  $n$  of the  $P$  and  $O_1^{(4)}$  lines are written as:

$$\Delta E^{\text{seg}}(P_n) = \Delta E_P^{\text{seg},0} + V_1(c_{P_{n-1}} + c_{P_{n+1}}) + 3V_2 \sum_{j=1}^2 (c_{O_{j,n}}^{(4)} + c_{O_{j,n-1}}^{(4)}) \quad (6)$$

$$\begin{aligned} \Delta E^{\text{seg}}(O_{1,n}^{(4)}) = & \Delta E_{O_1}^{\text{seg},0} + V_2(c_{P_n} + c_{P_{n+1}}) + V_3(c_{O_{1,n-1}}^{(4)} + c_{O_{1,n+1}}^{(4)}) \\ & + V_4 c_{O_{2,n}}^{(4)} + V_5(c_{O_{2,n-1}}^{(4)} + c_{O_{2,n+1}}^{(4)}) \end{aligned} \quad (7)$$

and the same as equation (7) for the  $O_2^{(4)}$  line inverting  $O_1^{(4)}$  and  $O_2^{(4)}$ . We solve the system of equations via a damped-dynamics algorithm (Berthier *et al* 2015), starting from a few different initial configurations. We can differentiate the solutions by calculating their free energy, which is straightforward in mean field. The equilibrium configuration is then the configuration of minimum free energy. Once the equilibrium composition is obtained, it is possible to cluster the sites of a given line to determine its average composition ( $c_P = (\sum_{n=1}^{100} c_{P_n})/100$  and  $c_{O_i}^{(4)} = (\sum_{n=1}^{100} c_{O_{i,n}}^{(4)})/100$ ), or to define different classes of sites. This is particularly interesting in the case of systems that tend to form ordered structures. Moreover the simplicity of the equations allows for segregation phenomena analysis presented below.

### 2.3. Monte Carlo simulations

To verify their accuracy, the mean-field calculations are complemented by Monte Carlo simulations, which are exact from a statistical physics point of view. We perform Metropolis Monte Carlo simulations in the grand canonical ensemble, which enables the optimization of both the number and distribution of the carbon atoms on the different sites.

The chemical potential,  $\mu$ , is calculated from the mean-field equation, which links  $\mu$  to the bulk concentration,  $c_{\text{bulk}}$ :

$$\mu = E_0 + k_B T \ln \frac{c_{\text{bulk}}}{1 - c_{\text{bulk}}}, \quad (8)$$

where  $E_0$  represents the incorporation energy of one isolated carbon atom into a bulk octahedral site. This expression neglects the interactions between carbon atoms in bulk, an approximation valid for bulk concentrations lower than 1000 appm as considered here.

Two types of events are considered. First, we introduce the incorporation/extraction of carbon atoms in order to optimize their concentration. A site is drawn randomly. If it is empty, the incorporation of one carbon atom is proposed and if it is occupied, extraction is proposed.

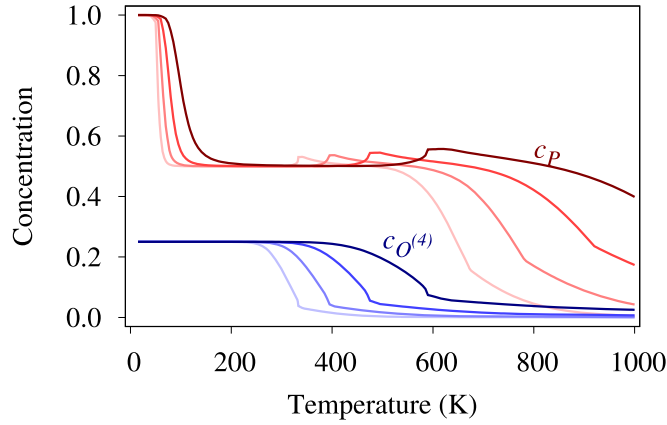


**Figure 3.** Evolution of  $c_P$  (in red) and  $c_{O^{(4)}}$  (in blue) concentrations with respect to temperature for  $c_{\text{bulk}} = 1, 10, 100$  and  $1000$  appm (from light to dark). The concentrations are obtained from the resolution of the mean-field equations per site.

The probabilities of incorporation and extraction are respectively:  $P_I = \frac{N_{\text{site}}}{N_C + 1} \exp - \frac{\Delta E_I - \mu}{k_B T}$  and  $P_E = \frac{N_C}{N_{\text{site}}} \exp - \frac{\Delta E_E + \mu}{k_B T}$ , with  $N_{\text{site}}$ , the total number of sites in the cell,  $N_C$ , the number of carbon atoms in the cell, and  $\Delta E_I$  (resp.  $\Delta E_E$ ), the energy variation related to the incorporation (resp. extraction) of an isolated carbon atom (Allen and Tildesley 1994) (computed from the variation of the system energy in equation (1) and adding or subtracting  $E_0$  when the carbon atom is either incorporated or extracted). The second type of event is the exchange between two sites. In that case, two sites, one of which is occupied by a carbon atom and the other empty, are drawn randomly. An occupation switch is then proposed with the probability  $P_{ij} = \exp - \frac{\Delta E_{ij}}{k_B T}$  ( $\Delta E_{ij}$  is the energy variation related to the exchange event) (Allen and Tildesley 1994). Finally, the probability to accept an event  $\alpha$  (incorporation, extraction, or exchange) is given by:  $\pi_\alpha = \min(1, P_\alpha)$ . In practice, we define a Monte Carlo macrostep as 5000 incorporation/extraction events followed by  $N_{\text{site}}$  exchange events. 7500 macrosteps are realized to converge to equilibrium. The cell is made up of the line of prismatic  $P$  sites and the six lines of octahedral  $O^{(4)}$  sites. 100 sites per line are considered as in the mean-field model ( $N_{\text{site}} = 700$ ) and periodic boundary conditions are used. Then the average over all the configurations provides access to the equilibrium concentration on each line.

### 3. Results

#### 3.1. Iso-concentrations in mean field

The evolution of the carbon concentration on the different segregation sites with respect to temperature is represented in figure 3 for several bulk concentrations that span the range of the Fe(C) solid-solution, i.e. for  $c_{\text{bulk}}$  from 1 to 1000 appm. The prismatic sites are more enriched in carbon than the  $O^{(4)}$  sites regardless of temperature. The prismatic sites are saturated ( $c_P = 1$ ) at very low temperature ( $< 100$  K). Above 100 K, there is a plateau at  $c_P = 0.5$  up to  $T = 500$ – $600$  K depending on the bulk concentration. For the  $O^{(4)}$  sites, a plateau is observed at  $c_{O^{(4)}} = 0.25$  up to 450 K. When the concentration of the  $O^{(4)}$  sites approaches zero, a non-monotonous variation of the concentration on the  $P$  sites is observed,

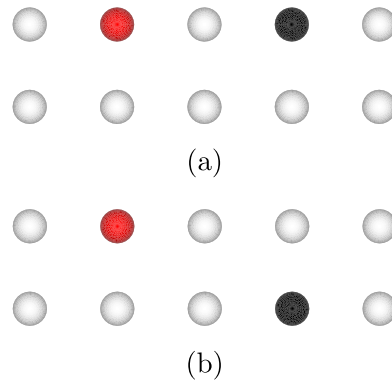


**Figure 4.** Schematic representation of the local arrangement of carbon atoms on a pair of  $O_1^{(4)}$  and  $O_2^{(4)}$  lines in the ground state. Once a first carbon atom is placed on a line (red sphere), a second carbon atom (black sphere) can be placed (a) on the same line or (b) on the other line, avoiding the neighbouring sites of the first atom.

while at higher temperature, an angular point is observed for both the prismatic and octahedral concentrations. Both features will be explained later in the text.

The concentration curves do not evolve significantly with respect to the bulk concentration. Quantitatively, a concentration increase from 1 to 1000 appm leads to: (i) an increase of the crossover temperature between the plateaus at  $c_P = 1$  and  $c_P = 0.5$  from 50 to 100 K; (ii) an increase of the end-of-plateau temperature for the  $O^{(4)}$  sites from about 300 to 450 K and correlatively an increase of the temperature corresponding to the small peak for the  $P$  sites; (iii) a slower decay with temperature of the concentrations on  $P$  and  $O^{(4)}$  sites after the plateaus at 0.5 for  $P$  and 0.25 for  $O^{(4)}$ ; (iv) an increase of both the concentration and the temperature at the angular point for both  $P$  and  $O^{(4)}$  sites.

The concentration of the octahedral sites is equal to 0.25 as the temperature tends towards zero. In view of the values for the segregation and the interaction energies used in the Ising model, it can be shown that the ground state corresponds to a concentration of 1 for the  $P$  sites and to a concentration of the octahedral sites equal to 0.25 resulting from a mixture of the two states represented in figures 4(a) and (b). These two states have the same energy and avoid all carbon–carbon repulsion: (i) one consists of an alternation of one in every two sites occupied by a carbon atom and an empty line forming the  $O^{(4)}$  pair (figure 4(a)) and (ii) one consists of an alternation of one in every four sites occupied by a carbon atom on each of the  $O^{(4)}$  lines (figure 4(b)). As a result, in the ground state there is a succession of sites that are simultaneously empty on the two lines, and of one occupied site on one of the two lines. Therefore we can define two sub-lattices  $\alpha$  and  $\beta$  of every other site for each line. The  $\beta$  sub-lattice has a null value both for  $O_1^{(4)}$  and  $O_2^{(4)}$  lines. The sites of the  $\alpha$  sub-lattice have a probability equal to 0.5 to be occupied but in a disordered manner, resulting in an average concentration of the  $\alpha$  sub-lattice equal to 0.5. The intra-line and inter-line order (i.e. empty  $\beta$  sites) is accompanied by an intra-line disorder related to the disorder of  $\alpha$  sub-lattice. In the following, the ordered state will refer, somewhat imprecisely, to the low-temperature state. Mean field enables the analysis of different regimes, as well as the non-monotonous behaviour of the  $P$  site concentration with respect to temperature. This requires to determine the concentrations per sub-lattice (figure 5). The plateaus for  $P$  and  $O^{(4)}$  result from the stability of the following ordered structures: (i) for the  $P$  line, this corresponds to the occupation of every other site along the line; (ii) the two nearest-neighbour  $O^{(4)}$  lines (figure 1) adopt the same

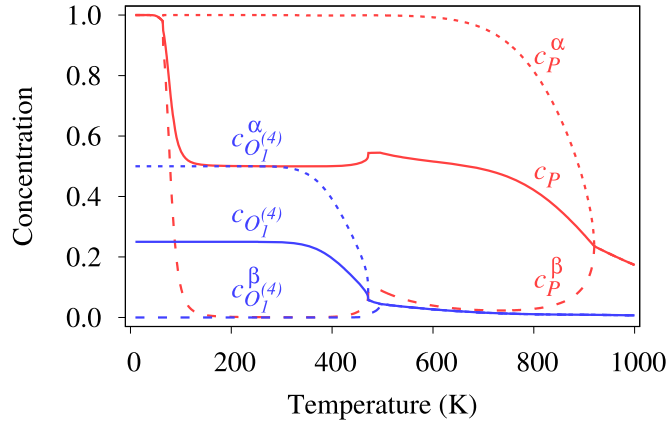


**Figure 5.** Evolution of the concentration of the prismatic  $P$  sites (in red:  $c_P$  in solid line,  $c_P^\alpha$  in dotted line and  $c_P^\beta$  in dashed line) and of the concentration of the octahedral  $O_1^{(4)}$  sites (in blue:  $c_{O_1^{(4)}}$  in solid line,  $c_{O_1^{(4)}}^\alpha$  in dotted line and  $c_{O_1^{(4)}}^\beta$  in dashed line) with respect to temperature for  $c_{\text{bulk}} = 100$  apm. All the octahedral lines behave as the  $O_1^{(4)}$  line. The concentrations are obtained from the resolution of the mean-field equations per site.

configuration, i.e.  $\beta$  sub-lattice is empty and  $\alpha$  sub-lattice is disordered with a concentration equal to 0.5. To conclude, the order on  $P$  sites is intra-line, whereas the order on  $O^{(4)}$  sites is both intra-line and inter-line. For a bulk concentration of 100 apm (figure 5), the prismatic site line is ordered between 80 and 940 K and the intra-line and inter-line order for the octahedral site lines ranges from 0 to 480 K.

The ordered/disordered regimes can be clearly evidenced by looking at the evolution with temperature of the intra-line long-range order (LRO) parameter,  $\eta = c_P^\alpha - c_P^\beta$  for the  $P$  line and  $\eta = 2(c_{O_1^{(4)}}^\alpha - c_{O_1^{(4)}}^\beta)$  for the  $O_1^{(4)}$  lines (figure 6). The intra-line order parameter for the  $P$  sites is equal to zero at low temperature (because  $c_P$  is close to 1 and we have a disordered state of empty sites along the dislocation line) and to 1 between 100 and 600 K during the plateau at  $c_P = 0.5$  before decreasing at higher temperatures when the line is depleted. Therefore the  $P$  line is successively disordered, ordered and disordered as a function of temperature. Regarding  $O^{(4)}$  lines, the intra-line LRO parameter shows a perfect order at low temperature and a totally disordered state well before the  $P$  line becomes disordered again. The inter-line order for the octahedral sites,  $\eta = \sum_n |c_{O_{1,n}^{(4)}}^\alpha - c_{O_{2,n}^{(4)}}^\alpha|/n$  coincides with the intra-line order. This is because at low temperature, whether in state of figure 4(a) or in state of figure 4(b), when  $c_{O_{1,n}^{(4)}}^\alpha = 0$ ,  $c_{O_{2,n}^{(4)}}^\alpha = 1$  and vice versa.

To summarize, the mean-field calculations evidence a very low temperature domain where the  $P$  line is disordered whereas  $O^{(4)}$  lines are ordered (both intra and inter-line LRO), and then a domain, where all lines are ordered (intra-line order for the  $P$  line and both intra-line and inter-line orders for the  $O^{(4)}$  lines). Order on the  $O^{(4)}$  lines disappears at a lower temperature than for the  $P$  line. An increase of the bulk concentration from 1 to 1000 apm increases both the intra-line ordering temperature for the  $P$  line and the disordering temperature for both the  $P$  and  $O^{(4)}$  lines.

In order to evidence that the non-monotony in the concentration of the  $P$  sites is due to the decrease of the  $c_{O_1^{(4)}}^\alpha$  concentration, we calculate the concentration evolution of the  $P$  line

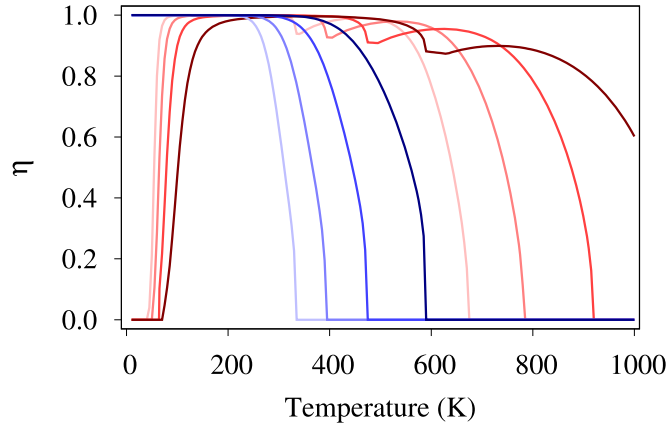


**Figure 6.** Evolution as a function of temperature of the intra-line LRO parameter for the  $P$  line,  $\eta = c_P^\alpha - c_P^\beta$  (in red), and for the  $O_1^{(4)}$  line,  $\eta = 2(c_{O_1^{(4)}}^\alpha - c_{O_1^{(4)}}^\beta)$  (in blue) for  $c_{\text{bulk}} = 1, 10, 100$  and  $1000$  appm (from light to dark). The inter-line  $O_1^{(4)} - O_2^{(4)}$  short-range order (SRO) parameter,  $\eta = \sum_n |c_{O_{1,n}^{(4)}}^\alpha - c_{O_{2,n}^{(4)}}^\alpha|/n$  coincides with the intra-line LRO parameter of the octahedral sites.

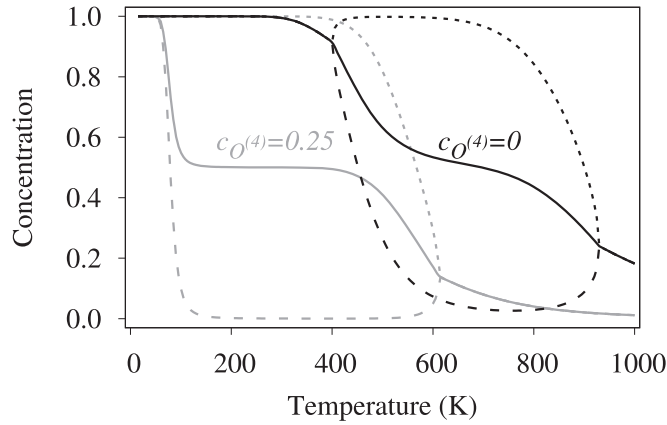


**Figure 7.** Evolution as a function of temperature of the concentration of prismatic sites when the concentration of octahedral lines is equal either to zero (in black) or to 0.25 (in grey) with  $c_{\text{bulk}} = 100$  appm.  $c_P$  is represented by a solid line,  $c_P^\alpha$  by a dotted line and  $c_P^\beta$  by a dashed line. The concentrations are obtained from the resolution of the mean-field equations per site.

imposing either empty  $O^{(4)}$  lines ( $c_{O^{(4)}} = 0$ ) or a concentration equal to 0.25 on the  $O^{(4)}$  lines (i.e. with a perfect intra-line and inter-line LRO) (figure 7). For  $c_{O^{(4)}} = 0$ ,  $c_P = 1$  up to about 400 K and then decreases monotonically. In the absence of segregation on the  $O^{(4)}$  lines, and despite the presence of LRO on the  $P$  line, there is no plateau at  $c_P = 0.5$  for the  $P$  sites. We recover here the results obtained when only  $P$  sites were considered as segregation sites in the dislocation core (Ventelon *et al* 2015). For  $c_{O^{(4)}} = 0.25$ ,  $c_P$  decreases monotonously with temperature again, but now the  $P$  line presents a plateau at  $c_P = 0.5$  as in the full calculation

(figure 5). Therefore, when the concentration of octahedral sites is constant (equal to either 0 or 0.25), the concentration of the prismatic sites does not present a peak.

The temperature increase is the driving force for the decrease of  $c_{O(4)}^\alpha$  at the end of the plateau. This leads to an increase of  $c_P^\beta$ , and in turn of  $c_P$ , because of the repulsive interactions between  $P$  and  $O(4)$  sites; the subsequent decrease of  $c_P^\beta$  is then due to the temperature increase. In order to describe these competitive effects of the temperature, we check that, in the case where segregation on  $O(4)$  lines is promoted (resp. not promoted) by increasing (resp. decreasing) the value of  $|\Delta E_{O(4)}^{\text{seg},0}|$ ,  $c_{O(4)}^\alpha$  decreases at higher temperatures (resp. lower temperatures) and the peak of  $P$  sites is less (resp. more) pronounced. This analysis shows that the non-monotonous behaviour of the segregation evolution of the  $P$  sites is due to the concentration variation of the  $O(4)$  lines. We also note that segregation is all the more important on the  $P$  line that the  $O(4)$  lines are little enriched (figure 7), which is perfectly consistent with the repulsion of carbon atoms between these lines.

The sub-lattice definition from the results obtained with the mean-field approach enables to simplify our model by forcing the same concentration on all the sites of each sub-lattice. It is also possible to force the absence of intra-line or inter-line order by imposing the same concentration on different sub-lattices. This means decreasing the number of equations considered in the model, which allows to predict the transition temperatures between two successive plateaus with respect to bulk concentration:

- The transition from  $c_P = 1$  to  $c_P = 0.5$  is related to the decrease of  $c_P^\beta$  from 1 to 0 with  $c_P^\alpha = 1$  and  $c_{O(4)} = 0.25$ . The system can be reduced to one equation that describes the evolution of  $c_P^\beta$  and the temperature at which  $c_P^\beta = 0.5$  is given by:  $T(c_P^\beta = 0.5) = (\Delta E_P^{\text{seg},0} + 2V_1 + 3V_2) / (k_B \ln \frac{c_{\text{bulk}}}{1 - c_{\text{bulk}}})$ . The transition temperatures  $T(c_P^\beta = 0.5) = 54$  K for  $c_{\text{bulk}} = 1$  appm and  $T(c_P^\beta = 0.5) = 101$  K for  $c_{\text{bulk}} = 1000$  appm are in perfect agreement with the full calculation.
- The transition from  $c_P = 0.5$  to  $c_P = 0$  is related to the decrease of  $c_P^\alpha$  from 1 to 0 with  $c_P^\beta \approx 0$  and  $c_{O(4)} \approx 0$ . In that case an approximate value of the transition temperature is given by:  $T(c_P^\alpha = 0.5) \approx \Delta E_P^{\text{seg},0} / (k_B \ln \frac{c_{\text{bulk}}}{1 - c_{\text{bulk}}})$ , resulting in  $T(c_P^\alpha = 0.5) \approx 940$  K for  $c_{\text{bulk}} = 100$  appm. Agreement with the full calculation is better for smaller bulk concentrations.
- The transition from  $c_{O(4)} = 0.25$  to  $c_{O(4)} = 0$  is related to the decrease of  $c_{O(4)}^\alpha$  from 0.5 to 0 with  $c_P^\beta \approx 0$ ,  $c_P^\alpha \approx 1$  and  $c_{O(4)}^\beta \approx 0$ . The transition temperature is determined by locally looking at an occupied site  $n$  of sub-lattice  $\alpha$ :  $T(c_{O(4)}^\alpha = 0.5) = (\Delta E_{O(4)}^{\text{seg},0} + V_2) / (k_B \ln \frac{c_{\text{bulk}}}{1 - c_{\text{bulk}}})$ . Then for a bulk concentration of 1 appm (resp. 1000 appm), the transition temperature is equal to 310 K (resp. 579 K), again in agreement with the full calculation.

The order/disorder critical temperatures for  $P$  sites ( $T_c^P$ ) and  $O(4)$  sites ( $T_c^{O(4)}$ ), which correspond to the angular points observed in figure 3, can also be estimated by considering that at the critical point: (i)  $c_{O(4)}^\alpha = c_{O(4)}^\beta = 0$  and  $c_P^\alpha = c_P^\beta = c_P$  for the  $P$  line and (ii)  $c_P^\alpha = 1$ ,  $c_P^\beta = 0$  and  $c_{O(4)}^\alpha = c_{O(4)}^\beta = c_{O(4)}$  for the  $O(4)$  lines. Thus at the critical point, the segregation energies can be written as: (i)  $\Delta E_P^{\text{seg}} = \Delta E_P^{\text{seg},0} + 2V_1 c_P$  for the  $P$  line (from equation (6)) and (ii)  $\Delta E_{O(4)}^{\text{seg}} = \Delta E_{O(4)}^{\text{seg},0} + V_2 + (2V_3 + V_4 + 2V_5)c_{O(4)}$  for the  $O(4)$  lines (from equation (7)). Resolution of (i) equation (4) and equation:  $T_c^P = 2V_1 c_P (1 - c_P) / k_B$  for the  $P$

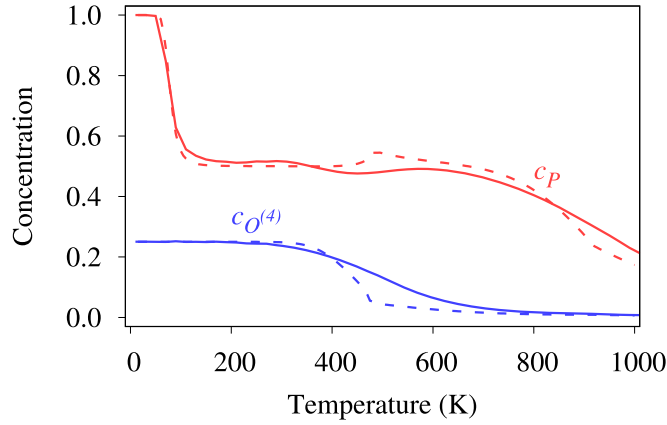


**Figure 8.** Evolution of the concentrations  $c_P$  (in red) and  $c_{O^{(4)}}$  (in blue) with respect to temperature for  $c_{\text{bulk}} = 100$  appm obtained in Monte Carlo (solid line) and in mean field (dashed line).

line and of (ii) equation (5) and equation:  $T_c^{O^{(4)}} = (2V_3 + V_4 + 2V_5)c_{O^{(4)}}(1 - c_{O^{(4)}})/k_B$  for the  $O^{(4)}$  lines gives values in very good agreement with simulations.

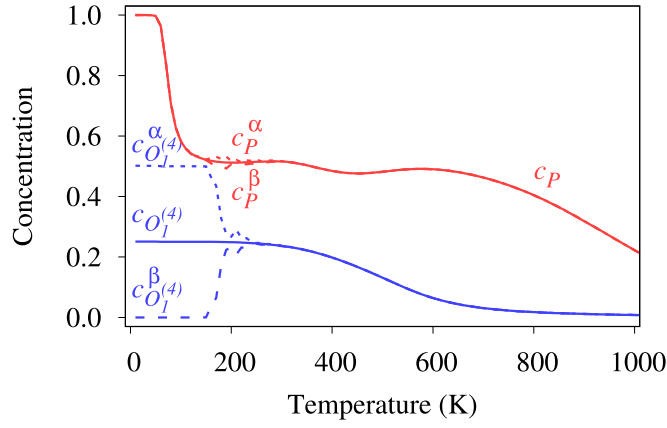
In summary, the mean-field calculations predict a higher segregation on the  $P$  line than on the  $O^{(4)}$  lines at all temperatures. The iso-concentrations present plateaus for both the  $P$  and  $O^{(4)}$  lines, which correspond to the stability of ordered structures. At very low temperature, the  $P$  line is saturated while the  $O^{(4)}$  lines are ordered with an average composition equal to 0.25. Order on the  $O^{(4)}$  lines is intra-line with a sub-lattice of empty sites and a disordered sub-lattice with equiatomic composition on the two lines; since carbon atoms avoid any C–C repulsion given our model, order is also inter-line. The  $P$  line is successively disordered, ordered and disordered as the temperature increases. The order/disorder critical temperature for the  $O^{(4)}$  lines is lower than that for the  $P$  line.

### 3.2. Comparison between mean field and Monte Carlo

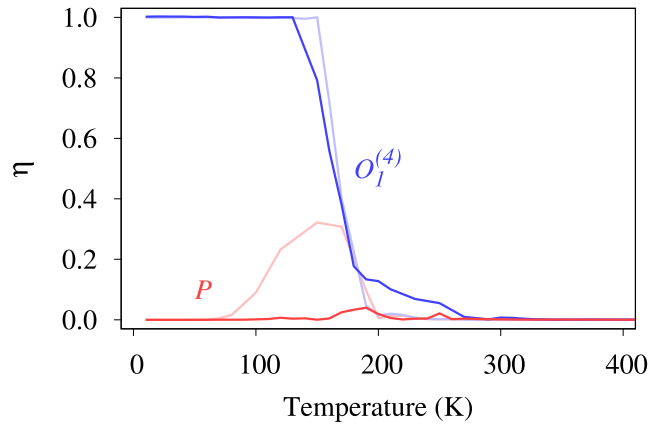
In this section, we compare the results obtained with the mean-field approach to those obtained with Monte Carlo simulations. Qualitatively, the iso-concentrations obtained with both approaches are very similar (figure 8). However we note that  $c_{O^{(4)}}$  decreases more gradually in Monte Carlo than in mean field and that the concentration for prismatic sites in Monte Carlo does not present a peak at the end of the plateau like in mean field, but rather weak oscillations.

In order to understand the origin of the differences between both resolution methods, we represent the concentration evolution per sub-lattice (figure 9(a)) and the intra-line LRO (figure 9(b)) obtained with Monte Carlo.

For  $c_{\text{bulk}} = 1$  appm, an order appears on the  $P$  sites between 150 and 200 K, and the intra-line order on the  $O^{(4)}$  sites starts to disappear a little before the intra-line order on the  $P$  sites (figure 9(b)). The order/disorder critical temperature for the  $O^{(4)}$  sites slightly increases with bulk concentration (figure 9(b)). When order disappears for the octahedral sites (and for the prismatic sites at  $c_{\text{bulk}} = 1$  appm), the  $c_{O^{(4)}}$  and  $c_P$  concentrations start to decrease with temperature. While in mean field, this decrease is coupled to the temperature increase and to the end of order, in Monte Carlo the decrease of  $c_{O^{(4)}}$  is solely due to the temperature increase in a disordered solution. The intra-line order of octahedral sites disappears at a lower



(a)



(b)

**Figure 9.** (a) Evolution of the concentration of the prismatic  $P$  sites (in red:  $c_P$  in solid line,  $c_P^\alpha$  in dotted line and  $c_P^\beta$  in dashed line) and of the concentration of the octahedral  $O_1^{(4)}$  line (in blue:  $c_{O_1^{(4)}}$  in solid line,  $c_{O_1^{(4)}}^\alpha$  in dotted line and  $c_{O_1^{(4)}}^\beta$  in dashed line) with respect to temperature for  $c_{\text{bulk}} = 100$  appm obtained in Monte Carlo. (b) Evolution with respect to temperature of the intra-line  $P$  LRO:  $\eta = c_P^\alpha - c_P^\beta$  (in red) and of the intra-line  $O_1^{(4)}$  LRO:  $\eta = 2(c_{O_1^{(4)}}^\alpha - c_{O_1^{(4)}}^\beta)$  (in blue) for  $c_{\text{bulk}} = 1$  appm (light) and 100 appm (dark) obtained in Monte Carlo.

temperature than in mean field, i.e. at about 220 K instead of 450 K (figure 6). The disappearance of order on the octahedral lines is not accompanied by a noticeable variation of  $c_{O_1^{(4)}}$ , but it induces a weak modulation on the  $P$  sites. Another modulation on the  $P$  sites appears when the concentration of the octahedral sites (disordered in Monte Carlo) decreases (at the inflection point on  $c_{O_1^{(4)}}$ , near 500 K in figure 9(a)). However, since the variation of  $c_{O_1^{(4)}}$  is gradual, this merely results in a modulation and not a peak on the concentration of the prismatic sites.



For  $c_{\text{bulk}} = 100$  appm, while the  $P$  line is ordered in mean field, there is no order in Monte Carlo. This is reflected in the fact that  $c_P^\alpha \approx c_P^\beta \approx c_P$  in figure 9(a). The presence of a very weak LRO in Monte Carlo compared to mean field is a very general result. Indeed the mean-field critical temperature is overestimated compared to the exact calculation obtained in Monte Carlo and the effect is maximum for a one-dimensional system (Ducastelle 1991). One would expect that the critical temperature of the  $P$  line is equal to zero as in a one-dimensional system. In fact the  $P$  line is not a perfect one-dimensional system because it is coupled to the  $O^{(4)}$  lines.

#### 4. Summary and conclusions

In this paper we describe the equilibrium segregation of interstitial carbon atoms in the core of  $1/2\langle 111 \rangle$  screw dislocations in bcc Fe using a generalized Ising model parametrized on DFT calculations. This Ising model is solved using mean-field calculations and Monte Carlo simulations to calculate the temperature dependence of the carbon concentration in the different segregation sites.

We demonstrate that the carbon enrichment is not limited to the prismatic sites forming the very core of the reconstructed dislocation because other sites around the prismatic line are attractive for carbon solutes in Fe according to our DFT calculations, namely the fourth neighbour octahedral sites of the reconstructed core. Their binding energy is similar to that of the prismatic core sites. The other sites up to sixth nearest neighbours are either unstable or repulsive for carbon atoms. On the basis of our DFT results, we developed an Ising Hamiltonian, which takes into account both the prismatic core sites and the fourth neighbour octahedral sites around the reconstructed core. Seven parameters are used in the Hamiltonian and fitted to DFT calculations: the two segregation energies on the prismatic site ( $-0.84$  eV) and on the octahedral site ( $-0.51$  eV) and five interaction terms that are all repulsive: the intra-line interactions, i.e. along the prismatic line ( $0.22$  eV) and along the octahedral line ( $0.30$  eV), as well as the inter-line interactions, i.e. between prismatic and octahedral sites ( $0.11$  eV) and between octahedral sites of two nearest-neighbour lines either in the same  $(111)$  plane or in the  $(111)$  plane just above or equivalently below ( $0.41$  eV).

In the range of bulk carbon concentrations from 1 to 1000 appm, we evidence that the segregation on the prismatic sites is more important than on the fourth neighbour octahedral sites, at all temperatures. At very low temperature ( $<100$  K), the prismatic line is saturated ( $c_P = 1$ ) and above, a plateau at  $c_P = 0.5$  appears up to 500–600 K depending on the bulk concentration. For the octahedral sites, a plateau is observed at  $c_{O^{(4)}} = 0.25$  up to 300–450 K. We evidence a temperature domain, between 300–450 K and 500–600 K, where every other site of the prismatic line is occupied by a carbon atom while the octahedral sites are empty. The mean-field calculations and Monte Carlo simulations lead to qualitatively comparable average concentrations on both the prismatic and octahedral sites. We note that the disappearance of order on the octahedral lines occurs at a lower temperature in Monte Carlo than in mean field, while there is little to no order on the prismatic line in Monte Carlo, depending on the bulk concentration. We also find that the concentration of the octahedral sites decreases more gradually in Monte Carlo than in mean field, which in turn leads to a weak modulation of the concentration of the prismatic sites instead of the pronounced peak evidenced in mean field.

This work is relevant to the dynamical strain ageing domain (between 400 and 600 K), where plasticity in Fe(C) alloys is unexpectedly controlled by the motion of screw dislocations (Caillard and Bonneville 2015), as in the low temperature regime in pure Fe

(Caillard 2010). At these high temperatures, carbon atoms are mobile and can segregate on the dislocation cores. Our model shows however that in this temperature regime, the dislocation is not fully decorated, but only half of the prismatic line is occupied by a carbon atom. Accounting for the half-occupation of the core sites will be essential in order to understand quantitatively the resulting dislocation mobility.

## Acknowledgments

This work was performed using HPC resources from GENCI-CINES computer center under Grant No. 2016-096821 and from PRACE (Partnership for Advanced Computing in Europe) access to SODIFE project. The authors acknowledge support from the ANR project DeGAS (ANR-16-CE08-0008). DR acknowledges support from LABEX iMUST (ANR-10-LABX-0064) of Université de Lyon (programme Investissements d'Avenir, ANR-11-IDEX-0007). This work has been carried out within the framework of the EUROfusion Consortium and has received funding from the Euratom research and training programme 2014–2018 under Grant Agreement No. 633053. The views and opinions expressed herein do not reflect those of the European Commission.

## ORCID iDs

F Berthier  <https://orcid.org/0000-0003-3564-3930>

L Ventelon  <https://orcid.org/0000-0001-9846-197X>

## References

- Allen M T and Tildesley D J 1994 *Computer Simulations of Liquids* (Oxford: Clarendon)
- Berthier F, Tadjine A and Legrand B 2015 *Phys. Chem. Chem. Phys.* **17** 28193–9
- Blöchl P E 1994 *Phys. Rev. B* **50** 17953
- Caillard D 2010 *Acta Mater.* **58** 3493–503
- Caillard D and Bonneville J 2015 *Scr. Mater.* **95** 15–8
- Chockalingam K, Janisch R and Hartmaier A 2014 *Modelling Simul. Mater. Sci. Eng.* **22** 075007
- Christian J W 1983 *Metall. Trans. A* **14** 1237–56
- Cottrell A H and Bilby B A 1949 *Proc. Phys. Soc. A* **62** 49
- Creuze J, Berthier F, Tétot R and Legrand B 2000 *Phys. Rev. B* **62** 2813–24
- Ducastelle F 1991 *Order and Phase Stability in Alloys* (Amsterdam: North-Holland)
- Fowler R H and Guggenheim E H 1960 *Statistical Thermodynamics* (London: Cambridge University Press)
- Hirth J P and Lothe J 1982 *Theory of Dislocations* (New York: Wiley)
- Kresse G and Furthmüller J 1996 *Phys. Rev. B* **54** 11169
- Kresse G and Joubert D 1999 *Phys. Rev. B* **59** 1758
- Lüthi B, Ventelon L, Elsässer C, Rodney D and Willaime F 2017 *Modelling Simul. Mater. Sci. Eng.* **25** 084001
- Lüthi B, Ventelon L, Rodney D and Willaime F 2018 *Comput. Mater. Sci.* **148** 21
- Rodney D, Ventelon L, Clouet E, Pizzagalli L and Willaime F 2017 *Acta Mater.* **124** 633
- Veiga R G A, Goldenstein H, Perez M and Becquart C S 2015 *Scr. Mater.* **108** 19–22
- Veiga R G A, Perez M, Becquart C S, Clouet E and Domain C 2011 *Acta Mater.* **59** 6963–74
- Ventelon L, Lüthi B, Clouet E, Proville L, Legrand B, Rodney D and Willaime F 2015 *Phys. Rev. B* **91** 220102(R)
- Ventelon L, Willaime F, Clouet E and Rodney D 2013 *Acta Mater.* **61** 3973
- Vitek V 1974 *Cryst. Lattice Defects* **5** 1–34
- Waseda O, Veiga R G A, Morthomas J, Chantrenne P, Becquart C S, Ribeiro F, Jelea A, Goldenstein H and Perez M 2017 *Scr. Mater.* **129** 16–9